Contrib Mineral Petrol (2002) 142: 714–723
DOI 10.1007/s00410-001-0318-5

Geoffrey D. Bromiley · Alison R. Pawley

The high-pressure stability of Mg-sursassite in a model hydrous peridotite: a possible mechanism for the deep subduction of significant volumes of H_2O

Received: 9 May 2001 / Accepted: 26 September 2001 / Published online: 13 November 2001

Abstract The stability of the high-pressure phase Mg-sursassite, previously MgMgAl-pumpellyite, in ultramafic compositions has been determined in experiments in the system $MgO–Al_2O_3–SiO_2–H_2O$ (MASH). The breakdown of Mg-sursassite + forsterite + enstatite to pyrope + vapour with increasing temperature was bracketed at 6.0 and 7.0 GPa. Below 6.0 GPa, Mg-sursassite + forsterite + vapour reacts to chlorite + enstatite. This reaction provides a mechanism for transfer of water from chlorite- to Mg-sursassite-bearing assemblages. At pressures of 7.0 GPa and above, the assemblage Mg-sursassite + phase A + enstatite was found. Phase relations involving Mg-sursassite and phase A are considered. For bulk compositions with a low water content, the vapour-absent reaction Mg-sursassite + forsterite = pyrope + phase A + enstatite determines the upper-pressure stability of Mg-sursassite, and provides a mechanism for the complete transfer of water from Mg-sursassite to phase A-bearing assemblages. Mg-sursassite plays an important role in peridotite compositions in the subducting slab because, at temperatures below 700 °C, it can transfer water from hydrous phases such as antigorite and chlorite to high-pressure stable phases such as phase A.

Introduction

The high-pressure hydrous phase Mg-sursassite [$Mg_5Al_5Si_6O_{21}(OH)_7$], previously known as MgMgAl-pumpellyite, was first synthesised by Schreyer et al. (1986) at 5.0 GPa, 700 °C. Schreyer et al. (1986) assumed this phase to be a Ca-free analogue of the MgAl-pumpellyite synthesised by Schiffman and Liou (1980), and termed the new phase MgMgAl-pumpellyite. The composition of this phase is close to that of a hydrated pyrope, and on the basis of preliminary work on its stability, Schreyer (1988) suggested that it could play an important role as a hydrous phase stable in a range of compositions under subduction zone conditions.

The crystal structure of $Mg_5Al_5Si_6O_{21}(OH)_7$ was reinvestigated using full-profile Rietveld analysis in two separate studies (Artioli et al. 1999; Gottschalk et al. 2000). Artioli et al. (1999) proposed a pumpellyite-type structure with a $P2_1/m$ space group showing extensive stacking disorder along the [001] direction (i.e. a pumpellyite-type structure with a certain amount of sursassite domains). In contrast, Gottschalk et al. (2000) demonstrated that the phase is, in fact, isostructural with Mn-sursassite, $Mn^{2+}{}_4Al_2Al_4[Si_6O_{22}(OH)_6]$, with Mg^{2+} replacing Mn^{2+} and one Al^{3+} replaced by $Mg^{2+} + H^+$. Gottschalk et al. (2000) also conducted a HRTEM investigation of the phase to support their crystal model, and proposed that the phase should be renamed Mg-sursassite.

The P–T stability field of Mg-sursassite in the system $MgO–Al_2O_3–SiO_2–H_2O$ (MASH) was determined in two preliminary studies by Schreyer (1988) and Liu (1989), and in a comprehensive study by Fockenberg (1998). Fockenberg (1998) demonstrated that Mg-sursassite is stable over a considerable temperature range from 3.4 to over 10 GPa, and suggested that it should be stable under subduction zone conditions in a range of compositions, including ultramafic compositions. However, as the composition of Mg-sursassite is significantly richer in Al and Si than normal ultramafic compositions, its stability in such compositions is unlikely to be determined by its stability in a bulk composition based on its own stoichiometry, as defined by Fockenberg (1998). Reactions determining the stability of Mg-sursassite, and other hydrous phases, in ultramafic

G.D. Bromiley (✉) · A.R. Pawley
Department of Earth Sciences, University of Manchester,
Oxford Road, Manchester M13 9PL, UK
E-mail: geoffrey.bromiley@uni-bayreuth.de

Present address: G.D. Bromiley
Bayerisches Geoinstitut,
Universität Bayreuth, 95440 Bayreuth, Germany

Editorial responsibility: W. Schreyer

compositions are listed in Table 1. Fockenberg (1998), Mysen et al. (1998) and Artioli et al. (1999) suggested that the high-temperature stability of Mg-sursassite will be determined, in ultramafic compositions, by reaction (1) (see Table 1). This implies that the stability of Mg-sursassite in peridotite compositions is defined by the stability of the pyrope-vapour tie-line.

Mysen et al. (1998) and Artioli et al. (1999) proposed consistent petrogenetic grids demonstrating how reaction (1) fits in with other reactions involving hydrous phases in peridotite compositions at high pressure. Both suggest that reaction (1) intersects reaction (2) (see Table 1), which marks the upper pressure stability of chlorite in peridotitic compositions. Artioli et al. (1999) determined phase relations for the phases MgMgAl-pumpellyite (Mg-sursassite), chlorite, pyrope, forsterite and enstatite in the MASH system using thermodynamic data from a variety of sources and the volume of MgMgAl-pumpellyite that they derived from Rietveld analysis of their synthetic samples. Figure 1 is based on Fig. 6 of Artioli et al. (1999) and shows the P–T slopes that they calculated. Intersection of reactions (1) and (2) results in an invariant point that governs the stability of Mg-sursassite towards lower pressures. The low-pressure stability of Mg-sursassite in ultramafic compositions is determined by the stability of the enstatite + chlorite + pyrope assemblage (Artioli et al. 1999), which will act as a 'compositional barrier' where forsterite is present, as shown by reaction (3).

Another reaction of possible importance is also shown in Fig. 1. On either side of the invariant point, the stability of chlorite towards higher pressure is defined by the stability of the chlorite + enstatite tie-line, which either breaks down to forsterite + pyrope through reaction (2), or breaks down to form forsterite + Mg-sursassite through reaction (4). Therefore, this reaction provides a mechanism for the formation of Mg-sursassite in subducting slabs following breakdown of chlorite-bearing assemblages, and thereby the transport of water in ultramafic parts of the subducting slab to significantly greater depths.

Artioli et al. (1999) suggested that only the vapour-absent reaction (3) has a positive slope. Reaction (1) was suggested to have a steep negative slope. The stability field of Mg-sursassite mapped out by Fockenberg (1998) was bounded by reactions with steep positive slopes. Because reaction (1) is expected to lie within the stability field of Mg-sursassite determined by Fockenberg (1998), this difference in P–T slope for the reactions implies that the stability of Mg-sursassite in peridotitic compositions should be significantly smaller than the stability based on its own stoichiometry. However, Mg-sursassite can still potentially play a pivotal role as a hydrous phase in peridotitic compositions because its stability field has been suggested to overlap that of chlorite towards lower pressures (Mysen et al. 1998), and could overlap that of other higher pressure hydrous phases towards higher pressures. Several dense hydrous magnesium silicates (DHMS) have been shown to be stable below 10 GPa and have stability fields that overlap that of Mg-sur-

Table 1 Important reactions considered in the text that determine the stability of Mg-sursassite, chlorite and phase A in ultramafic compositions in the system MASH

(1)	Mg-sursassite + forsterite + enstatite = pyrope + water
(2)	Chlorite + enstatite = pyrope + forsterite + water
(3)	Mg-sursassite + forsterite = enstatite + chlorite + pyrope
(4)	Chlorite + enstatite = Mg-sursassite + forsterite + water
(5)	Forsterite + water = phase A + enstatite
(6)	Mg-sursassite + forsterite = phase A + pyrope + enstatite
(7)	Mg-sursassite + phase A + enstatite = pyrope + vapour

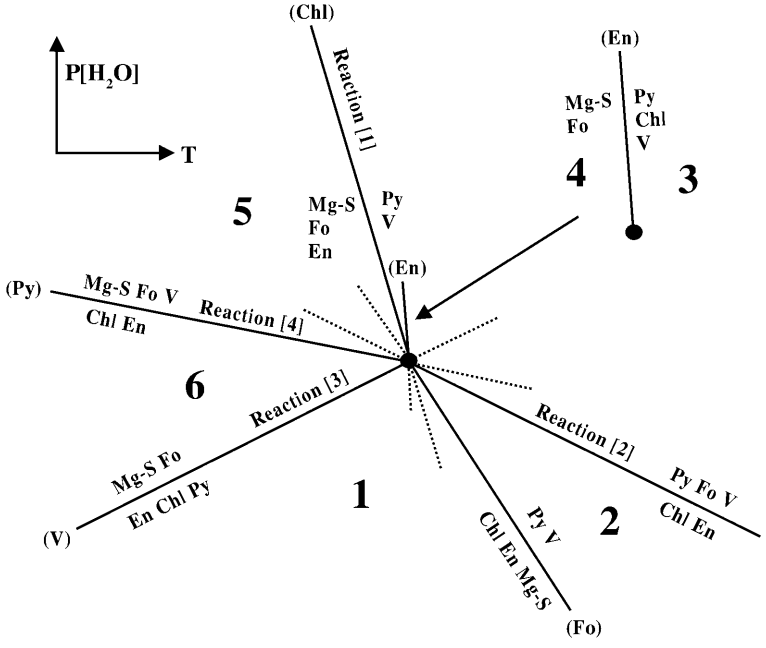

Fig. 1 Schreinemaker's web for the phases Mg-sursassite (*Mg-S*), chlorite (*Chl*), enstatite (*En*), forsterite (*Fo*), pyrope (*Py*) and vapour (*V*) in the system MASH, taken from Artioli et al. (1999)

sassite as determined by Fockenberg (1998). These include phase A (Luth 1995), clinohumite-OH and chondrodite-OH (Wunder 1998; Pawley 2000), and 10 Å phase (Chinnery et al. 1999).

Despite the possible importance of Mg-sursassite in the peridotite + vapour system, no experimental information is available on its high-pressure stability in this system. The aim of the present study was to experimentally determine the stability of Mg-sursassite in a model peridotite + vapour system under subduction zone conditions, and thereby to assess its importance as a hydrous phase in ultramafic parts of the subducting slab.

Experimental method

In order to determine the stability of Mg-sursassite in ultramafic compositions a series of high-pressure phase-equilibria experiments were performed.

Synthesis and characterisation of Mg-sursassite

Mg-sursassite was synthesised from a 5:2.5:6 mix of reagent grade brucite, corundum and finely ground quartz in three separate experiments. The starting mix was loaded into 5.08 mm o.d. Pt capsules that were then welded shut. Because of the high water content of the starting mix, no additional water was added. The capsules were loaded into sample assemblies for use in a multi-anvil device of the Walker design (Walker et al. 1990; Walker 1991). An Inconel foil furnace was used to maximise space inside the pressure medium. Tungsten-carbide anvils were used with a truncated edge length of 12 mm. Samples were run at 6.5 GPa, 550 °C for 48 h, and run products were identified optically and by powder X-ray diffraction (XRD). One of the samples was also prepared as a grain mount for analysis using a scanning electron microscope fitted with an energy-dispersive spectrometer (SEM-EDS) for quantitative analysis.

Water was released on piercing the retrieved capsules, indicating that the reaction had occurred. Run products were analysed by powder XRD using a Philips diffractometer with a copper filament running at 40 kV and 20 mA. XRD traces revealed that the starting mix had broken down to form Mg-sursassite with small amounts of coesite and topaz-OH [$Al_2SiO_4(OH)_2$]. No significant difference between the XRD peaks of different synthesis experiments was noted. Over 30 Mg-sursassite peaks in the traces were matched with peak data from Schreyer et al. (1991). Topaz-OH peaks were matched using data from Wunder et al. (1993). Because the starting mix used in the synthesis experiments had a bulk composition corresponding to that of Mg-sursassite, the presence of small amounts of topaz-OH and coesite indicates that the composition of the Mg-sursassite synthesised was slightly Mg-rich. SEM-EDS analysis of one of the run products was conducted using a JEOL 6400 SEM with an accelerating voltage of 15 keV, a probe current of 1.5×10^{-6} A and a working distance of 39 mm. Mg-surassite crystals were elongated, euhedral crystals of typically only a few microns in length (ranging up to 10 μm). The stoichiometry of the Mg-sursassite crystals was determined to be 5.28(11) MgO, 2.51(14) Al_2O_3 and 5.81(13) SiO_2. Point analysis of over 50 grains showed no significant variation in composition. Slight Mg-enrichment is in accordance with the formation of small amounts of coesite and topaz-OH. In contrast, Fockenberg (1998) synthesised slightly Al-rich Mg-sursassite.

Lattice parameters for Mg-sursassite were determined from XRD data. Refinement was carried out based on a monoclinic cell with space group A2/m, to allow comparison with the values of Schreyer et al. (1991) and Artioli et al. (1999). These values are given in Table 2. Values of cell parameters for the sample synthesised in the present study are in good agreement with the values for the sample synthesised by Schreyer et al. (1991). However, the parameters are noticeably smaller than the cell parameters for the sample synthesised by Artioli et al. (1999), especially the *a* and *c* parameters. Gottschalk et al. (2000) note that the values obtained by Artioli et al. (1999) are considerably different from those of samples synthesised in previous studies. Cell parameter data therefore suggest that the sample synthesised in the present study is Mg-sursassite, as opposed to a distorted pumpellyite structure as proposed by Artioli et al. (1999).

Phase equilibrium experiments

A series of experiments were conducted to determine the high-temperature stability of Mg-sursassite in ultramafic compositions as defined by reaction (1). Experiments were performed in the simplified end-member system $MgO–Al_2O_3–SiO_2–H_2O$ (MASH). A starting mix was made up of the synthetic Mg-sursassite and synthetic, pure Mg end-member enstatite, forsterite and pyrope. Enstatite and pyrope were synthesised from oxide mixes in a Boyd and England (1960) design piston-cylinder apparatus under the conditions listed below. The forsterite used was from a batch synthesised at Manchester by S.J. Kohn. Synthesised phases were examined optically and by XRD. Cell dimensions were determined from XRD peak data using UNITCELL (Holland and Redfern 1997) with a Si standard, and referenced using the following JCPDS cards.

Enstatite was synthesised at 2.0 GPa, 900 °C for 48 h from an oxide mix. The cell dimensions were $a = 9.606(5)$ Å, $b = 8.817(4)$ Å, $c = 5.171(5)$ Å, $\beta = 108.25(6)°$ and $V = 415.9(1)$ Å^3 (JCPDS card 35-0610). The XRD pattern of enstatite suggested that it was low clinoenstatite (P21/c), in agreement with Shinmei et al. (1999).

Pyrope was synthesised at 2.5 GPa, 900 °C for 48 h from an oxide mix. The cell dimension was $a = 11.455(3)$ Å (JCPDS card 15-0742).

The forsterite cell dimensions were determined as being $a = 5.983(3)$ Å, $b = 10.195(2)$ Å, $c = 4.754(2)$ Å and $V = 290.0(2)$ Å^3 (JCPDS card 34-0189).

A bulk composition for the starting mix corresponding to a model peridotite composition was chosen (Fig. 2), and consisted of a stoichiometric mix of the phases according to reaction (1), and subsequently enriched in forsterite and enstatite (bulk composition 3 MgO: 0.2 Al_2O_3: 2.2 SiO_2). The projection of this composition from the vapour apex of the MASH compositional tetrahedron lies within the 3-phase pyrope–enstatite–forsterite field (Fig. 2). Careful examination of the geometry of these phases in compositional space reveals that the bulk composition chosen can be used to bracket reaction (1) as long as a significant amount of excess water is always present. The reaction can be bracketed by determining the stabilities of Mg-sursassite- and pyrope-bearing assemblages (the assemblages Mg-sursassite + forsterite + enstatite + vapour and pyrope + forsterite + enstatite + vapour are stable in areas 4 and 5 of the Schreinemaker's plot shown in Fig. 1).

Aliquots of 6–7 mg of the starting mix were loaded into 2.5–3-mm-long 2-mm-o.d. Pt capsules with 20 wt% distilled water, and the capsules welded shut. Capsules were loaded into a sample

Table 2 Cell parameters for the phase $Mg_5Al_5Si_6O_{21}(OH)_7$ from the present study compared with values from Schreyer et al. (1991) and Artioli et al. (1999). *Numbers in parentheses* are standard deviations on the last quoted decimal place

Parameter	Present study	Schreyer et al. (1991)	Artioli et al. (1999)
a (Å)	8.547 (5)	8.544 (1)	8.5759 (4)
b (Å)	5.699 (3)	5.717 (1)	5.7295 (2)
c (Å)	18.452 (8)	18.491 (2)	18.5376 (9)
Beta (deg.)	97.63 (4)	97.75 (1)	97.691 (39)
Volume (Å^3)	890.7 (6)	893.4 (1)	902.66 (9)

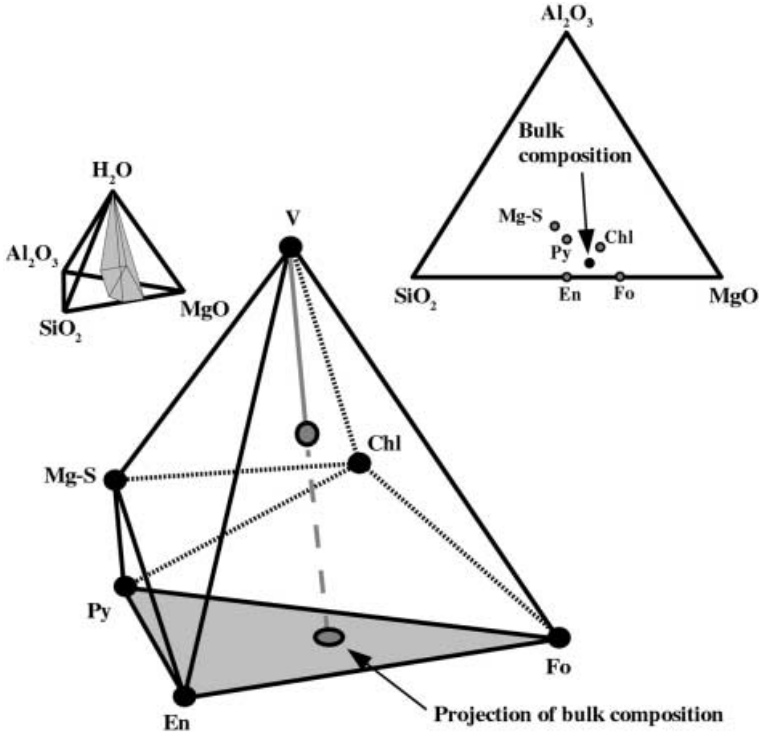

Fig. 2 Relationships between the phases considered in Fig. 1 in compositional space and the bulk composition chosen for experiments, shown in a ternary plot (projected from *V*) and in a 3-D view of part of the MASH tetrahedron (in the same orientation as the small MASH tetrahedron also shown). Vapour axis has been shortened

assembly for use in the Walker-type multi-anvil device. Heating was achieved using an internal graphite resistance furnace, and temperatures were measured using a Pt/Pt10%Rh (S-type) thermocouple. No correction for the effect of pressure on thermocouple e.m.f. was applied. For pressures up to 7 GPa, 12 mm truncated edge length (TEL) tungsten carbide anvils were used. For higher pressure runs, 8 mm TEL cubes were used. MgO ceramic octahedra with integral gaskets were used as pressure media. Pressure was calibrated at 1,000 °C using the quartz–coesite transition in SiO_2 (Bohlen and Boettcher 1982), the garnet–perovskite transformation in $CaGeO_3$ (Susaki et al. 1985), and the coesite–stishovite transition in SiO_2 (Yagi and Akimoto 1976). Pressure and temperature uncertainties, without taking into account the effect of pressure of thermocouple e.m.f., are estimated to be ±4% and ±20 °C respectively.

After quenching, recovered capsules were weighed, carefully pierced and reweighed to check for the presence of water. Water was clearly seen to be present in most runs when the capsules were pierced. Runs in which excess water was not noted were discounted. Run products were recovered and examined both optically and using XRD. Two run products were also prepared as powder mounts for examination using SEM (EDS).

Experimental results

Results of experiments to determine the high-pressure stability of Mg-sursassite in the peridotite + vapour analogue MASH system are listed in Table 3 and plotted in Fig. 3. Results are given in terms of the stable assemblage determined by comparison between the XRD patterns of run products and starting materials. In most cases, the reaction went to completion. In cases where the reaction did not go to completion, the amount of reaction was estimated from changes in peak heights. In all cases, except run PP9, run direction could be unequivocally discerned.

In experiment PP1, at 5.5 GPa, 660 °C, the assemblage chlorite + forsterite + enstatite was noted. No trace of Mg-sursassite from the starting mix was noted in the XRD pattern.

In experiments above 7.0 GPa and below 800 °C, and in both low-temperature experiments at 7.0 GPa (PP8 and APP1), the presence of an additional phase was inferred from the presence of a number of new peaks in XRD patterns. The appearance of this phase coincided with the disappearance of forsterite, an increase in enstatite, and a marked lowering of the amount of excess water contained in capsules after the experiments. Peak positions for this additional phase are in accordance with data for the dense hydrous magnesium silicate (DHMS) phase A [$Mg_7Si_2O_8(OH)_6$] first synthesised by Ringwood and Major (1967). However, the peaks are small and broad compared with peaks for the other phases present in the run products.

XRD data suggested that enstatite in all of the run products was low clinoenstatite ($P2_1/c$). Between 6.5 and 7.0 GPa, Shinmei et al. (1999) suggested that a phase transition occurs in clinoenstatite, from the low-pressure $P2_1/c$ to the high-pressure C2/c form. However, this transition is non-quenchable, and was not noted in the run products.

Averaged results of SEM-EDS analysis of the run products formed in APP1 and APP2 are given in Table 4. Analysis of APP1 revealed that the run products consisted of approximately 100-μm-diameter polycrystalline aggregates. These contained some individually distinguishable grains of enstatite and Mg-sursassite (and some relic pyrope), but mainly consisted of a cryptocrystalline intergrowth of grains that could not be

Table 3 Results of experiments to determine the stability of Mg-sursassite in the system MASH (peridotite + H_2O analogue)

Exp. no.	Pressure (GPa)	Temp. (°C)	Duration (h)	Results[a]	Notes[b]
PP1	5.5	660	52	Chl + Fo + En	No Mg-S left; minor Py left
PP2	5.5	700	62	Py + Fo + En	Complete reaction
PP5	6.0	660	53	Mg–S + Fo + En	50% reaction
PP6	6.0	690	54	Py + Fo + En	Complete reaction
PP7	6.0	720	60	Py + Fo + En	75% reaction
PP3	6.5	680	55	Mg–S + Fo + En	50% reaction
PP4	6.5	720	63.5	Py + Fo + En	Complete reaction
PP8	7.0	660	57	Mg–S + En + Ph–A	No Py or Fo left; large growth in En peaks
PP9	7.0	700	48	Py + Mg–S + Fo + En	No reaction in terms of Mg-S and Py; close to reaction curve
PP10	7.0	730	61	Py + Fo + En	Complete reaction
PP12	8.0	650	57	Mg–S + En + Ph–A	Complete reaction
PP11	8.0	700	50.5	Mg–S + En + Ph–A	Complete reaction
PP13	8.0	740	48	Py + En + PhA	Complete reaction
PP14	9.0	730	55	Mg–S + En + Ph–A	Complete reaction
PP15	9.0	770	47	Py + En + PhA	Complete reaction
APP1	7.0	630	49	Mg–S + En + PhA	SEM analysis
APP2	8.0	800	51	Py + Fo + En	SEM analysis

[a]Results are given in terms of the stable assemblage suggested on the basis of XRD peak height comparison
[b]Reaction given in terms of approximate change in peak heights

individually distinguished. Point analyses of this intergrowth revealed that it consisted of phase A, enstatite and Mg-sursassite. Individual analyses for the intergrowths are listed in Table 4. Analyses were performed by rastering the beam over a small area of the sample. The extremely small grain size of phase A in APP1 could explain why the XRD peaks for phase A in other run products are small and broad. Compositions of analysed Mg-sursassite grains were similar to the composition of Mg-sursassite used in the starting mix. Analysed enstatite grains contained a negligible amount of Al_2O_3.

SEM analysis of APP2 revealed the presence of enstatite, forsterite and pyrope only, with compositions close to ideal values, except enstatite, which contained small amounts of Al_2O_3 (less than 0.9 wt%). Grain size varied between 2 to 15 μm for all three phases, and there was no evidence of zoning. The absence of Mg-sursassite indicates complete reaction to the new assemblage (pyrope + enstatite + forsterite).

Discussion of experimental results

Reaction (1), the breakdown of Mg-sursassite with increasing temperature, was bracketed at 6.0 and 6.5 GPa (Fig. 3). If the reaction line is drawn so that it lies close to the data point PP9, in which both Mg-sursassite and pyrope were present, then the reaction has a large positive gradient. This is in contrast with the negative slope suggested by Artioli et al. (1999) based on thermodynamic calculation. However, the calculations of Artioli et al. (1999) assumed that the phase

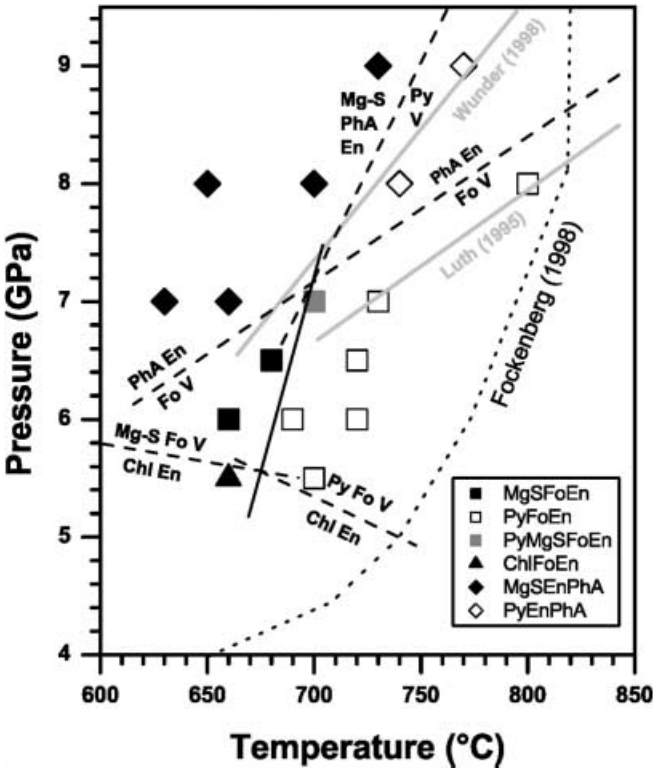

Fig. 3 Plot of results of experiments to determine the stability of Mg-sursassite in the system MASH (peridotite + V). *Broken lines* indicate reaction positions determined from unseeded runs. Positions of the reaction phase A + enstatite = forsterite + water determined by Luth (1995) and Wunder (1998) are shown in *grey*. Stability field of Mg-sursassite as determined by Fockenberg (1995) is shown as a *dotted line*

Table 4 SEM-EDS analysis of run products. Individual analyses for cryptocrystalline intergrowths (CI) of phase A, enstatite and Mg-sursassite noted in APP1 are listed. H_2O contents of hydrous phase are estimated from difference to 100 wt%

Exp. no.	Phase	Points	SiO_2		Al_2O_3		MgO		H_2O
			(wt%)	SD	(wt%)	SD	(wt%)	SD	
APP1	En	7	59.58	0.51	0.31	0.20	39.53	0.27	–
	Py	3	44.63	0.53	25.57	0.93	29.12	0.78	–
	Mg-S	3	40.01	0.56	28.25	0.51	23.31	0.52	7.9
	CI	1	37.96	–	10.73	–	41.92	–	9.4
	CI	1	57.39	–	1.44	–	39.73	–	1.4
	CI	1	43.05	–	9.10	–	40.89	–	6.7
	CI	1	39.62	–	10.52	–	41.06	–	8.8
	CI	1	45.23	–	7.60	–	40.06	–	7.1
	CI	1	46.88	–	7.01	–	40.47	–	5.6
	CI	1	38.69	–	12.08	–	39.12	–	10.0
	CI	1	38.27	–	10.54	–	41.24	–	9.1
	CI	1	55.32	–	2.61	–	39.5	–	2.6
	CI	1	39.04	–	11.68	–	40.51	–	8.8
	CI	1	44.91	–	10.85	–	37.31	–	6.9
	CI	1	52.6	–	3.68	–	39.98	–	3.7
	CI	1	43.15	–	14.63	–	34.19	–	8.0
	CI	1	44.48	–	12.86	–	34.68	–	7.9
	CI	1	43.30	–	8.32	–	40.30	–	8.1
	CI	1	42.47	–	9.86	–	40.13	–	7.5
	CI	1	40.79	–	10.41	–	41.30	–	7.5
	CI	1	39.9	–	11.68	–	39.66	–	8.8
	CI	1	39.78	–	11.23	–	40.14	–	8.9
	CI	1	50.45	–	9.25	–	35.14	–	5.2
APP2	Py	17	45.23	0.48	24.32	0.62	29.66	0.43	–
	Fo	6	42.48	0.42	0.16	0.07	56.50	0.38	–
	En	3	59.14	0.27	0.48	0.36	39.28	0.54	–

$Mg_5Al_5Si_6O_{21}(OH)_7$ had a distorted pumpellyite structure, and were based on data for a sample that Gottschalk et al. (2000) suggests differs significantly from samples synthesised in other studies.

At 5.5 GPa, 660 °C (PP1), the assemblage chlorite + forsterite + enstatite was noted (with small amounts of pyrope). This assemblage is stable in areas 1, 2 and 6 of the Schreinemakers' web shown in Fig. 1. The results of experiments PP1 and PP5 may, therefore, be tentatively used to locate the position of reaction (4), marking the low-pressure stability of Mg-sursassite. The position of this reaction is in good agreement with position estimated by Mysen et al. (1998). However, it should be noted that chlorite was not seeded in the starting mix. Chlorite growth in PP1 could have been metastable, and the results of experiments listed here cannot be considered a bracket for reaction (4). At 5.5 GPa and 700 °C the assemblage pyrope + forsterite + enstatite formed, as would be expected in area 3 of the Schreinemakers' web shown in Fig. 1.

The observed changes in phase proportions in higher pressure experiments where phase A formed are in accordance with reaction (5). This reaction was bracketed by Luth (1995) and Wunder (1998). For pressures above 7 GPa, the position of reaction (5) inferred in this study (as shown in Fig. 3) lies between the reaction positions determined by Luth (1995) and Wunder (1998). However, the gradient of reaction (5) shown in Fig. 3 is slightly smaller than suggested by Luth (1995) and significantly smaller than suggested by Wunder (1998). It should be noted, however, that phase A was not seeded in any of the experiments. It is possible that phase A growth was metastable, or that the stability field of Mg-sursassite relative to that of phase A was overestimated. The present results can only be used to provide an initial indication of the stability of Mg-sursassite relative to phase A. Therefore, within experimental uncertainties, the position of reaction (5) determined in the present study may be in agreement with both Luth (1995) and Wunder (1998).

Mg-sursassite stability in relation to the stability of phase A

Phase A is a DHMS first synthesised by Ringwood and Major (1967), and has been proposed as a storage site for H_2O in ultramafic compositions under subduction zone conditions. Pawley and Wood (1995) investigated the low-pressure stability of phase A and determined that, in SiO_2-poor compositions, it could crystallise at pressures below 6 GPa. Therefore, phase A is stable to pressures considerably lower than many other DHMS, which are only stable at pressures exceeding 10 GPa. Studies on the high-pressure phase relations of DHMS (e.g. Liu 1986; Kawamoto et al. 1995; Irifune et al. 1998) have shown that phase A has a large stability field at high pressure, and that it is stable to pressures greater than 15 GPa. At high pressure, the stability field of phase A overlaps that of other DHMS. Therefore, phase

A is one of the most important of the DHMS in terms of potential to transport water in ultramafic parts of subducting slabs.

The stability fields of Mg-sursassite and phase A in the system MASH (as an analogue for the peridotite + H_2O system) are expected, based on the studies of Fockenberg (1998), Luth (1995) and Wunder (1998), to overlap considerably, as both phases have extensive stability fields. However, Fockenberg (1998) discounted the significance of phase relations between Mg-sursassite and phase A because phase A had not been noted in previous studies on the stability of Mg-sursassite. Figure 4 is part of the MASH tetrahedron showing the relationships between Mg-sursassite, phase A, enstatite, forsterite, pyrope and water in compositional space. Figure 5 is a Schreinemaker's web drawn in accordance with the experimental results showing phase relations as a result of the intersection of reactions (1) and (5). The stable phase assemblages expected for peridotite compositions (i.e. bounded by the pyrope–enstatite–forsterite assemblage) containing additional amounts of water are also shown. These compatibility diagrams suggest that hydrous phase-bearing assemblages expected for typical mantle compositions with only a few weight percent water (i.e. where the assemblage pyrope + enstatite + forsterite is stable) are likely to differ from the phase assemblages seen in run products in the present study, where a large amount of excess water was always present. In run products from areas 2a and 3a of Fig. 5, the assemblage phase A + Mg-sursassite + enstatite was noted. However, this assemblage is only stable for unrealistically high water contents. For much lower water contents, the stable assemblage in area 2a is Mg-sursassite + pyrope + forsterite + enstatite (or Mg-sursassite + phase A + forsterite + enstatite), and the stable assemblage in area 3a is phase A + pyrope + forsterite + enstatite. Therefore, the vapour-absent reaction (6) is of critical importance in defining the upper-pressure stability of Mg-sursassite in ultramafic compositions with low water contents. This reaction is analogous to reaction (3), which defines the low-pressure stability of Mg-sursassite. In both instances, the Mg-sursassite–forsterite tie-line is broken by the formation of assemblages involving a hydrous phase (chlorite or phase A) with enstatite and pyrope. The phase relations shown in Fig. 5 therefore demonstrate that the presence of phase A greatly reduces the stability of Mg-sursassite in typical ultramafic compositions. However, as the breakdown of Mg-sursassite-bearing assemblages to phase A-bearing assemblages proceeds by the vapour-absent reaction (6), no water is lost. Unfortunately, the experimental data do not provide information on the position of reaction (6) because of the high water content of the bulk composition chosen. The position of this reaction can only be constrained at present by the positions of reactions (5) and (7).

The assemblage phase A + pyrope + enstatite + forsterite is stable over areas 3a and 4a; therefore, the range of temperatures over which water is tied up in hydrous phases is greatly increased relative to systems in which Mg-sursassite is the only stable hydrous phase at high-pressure. The considerable stability field of phase A at higher pressures (i.e. above 10 GPa) overlaps that of other DHMS in the systems MSH (Irifune et al. 1998) and MASH (Kawamoto et al. 1995). Transfer of water from Mg-sursassite- to phase A-bearing assemblages thereby provides a mechanism for the deep subduction of significant volumes of water in ultramafic material.

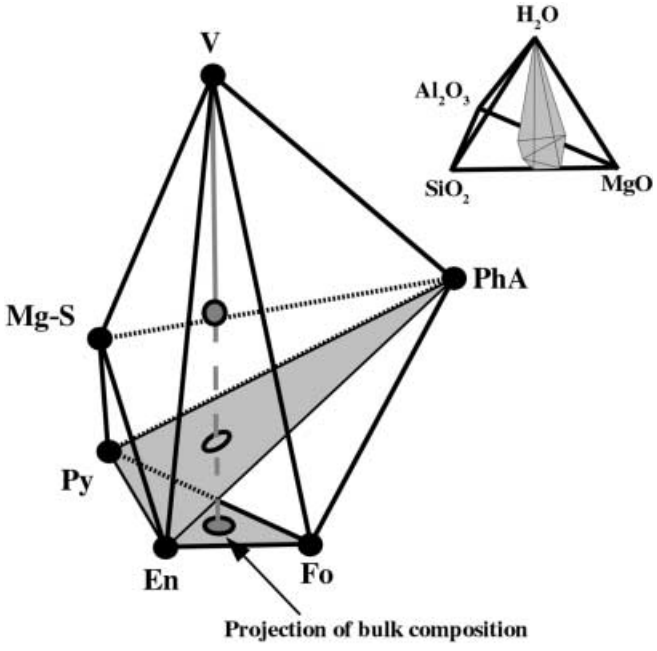

Fig. 4 Part of the MASH tetrahedron (in the same orientation as the small MASH tetrahedron also shown) showing relationships between the phases Mg-sursassite, pyrope, forsterite, enstatite, phase A (*PhA*) and vapour, and the bulk composition in compositional space. The vapour axis has been shortened and the geometry of the phases altered considerably for clarity. The plane phase A + pyrope + enstatite is *shaded* to demonstrate how formation of this assemblage [i.e. reaction (6), see Table 1] limits Mg-sursassite stability in ultramafic compositions with small amounts of water

For bulk compositions with a low water content, the assemblage pyrope + forsterite + enstatite coexists with either Mg-sursassite (areas 1a and 2a), phase A (areas 3a and 4a) or free fluid phase (areas 5a and 6a). For bulk compositions with slightly higher water contents (above 2 wt% for Mg-sursassite-bearing assemblages and above 2 to 6 wt% for phase A-bearing assemblages), the stable assemblages will be Mg-sursassite + enstatite + forsterite + vapour in area 1a, Mg-sursassite + phase A + forsterite + enstatite in area 2a, phase A + pyrope + enstatite + Mg-sursassite in area 3a and phase A + pyrope + enstatite + vapour in area 4a. Therefore, for these higher water contents, the size of the stability fields of phase A and Mg-sursassite are increased, and these two phases can form stable assemblages together.

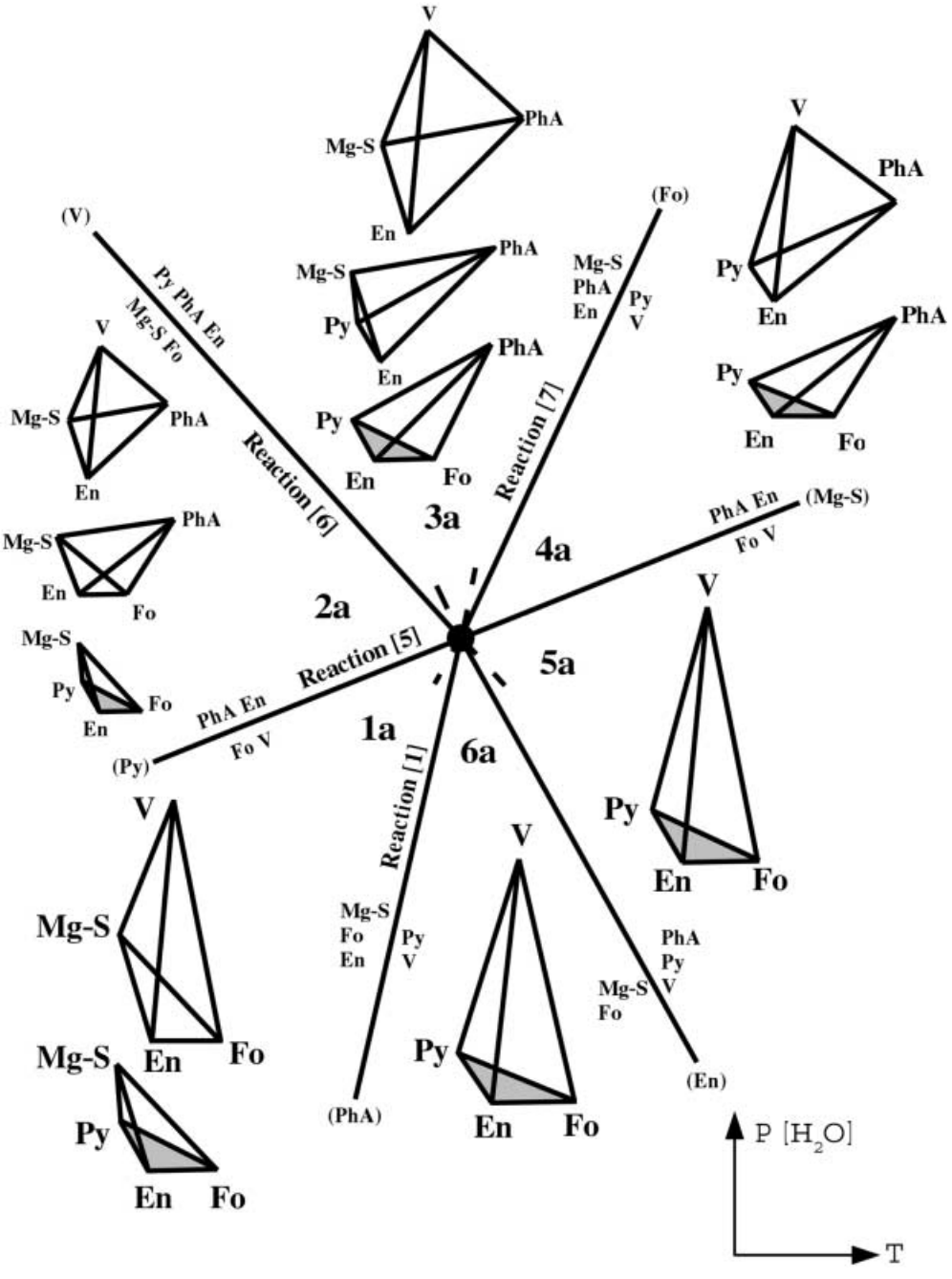

Fig. 5 Schreinemakers' web showing the relationship between the high-pressure stabilities of Mg-sursassite and phase A. The web is drawn in accordance with experimental results. Stable assemblages are shown for each of the labelled fields based on the polyhedron shown in Fig. 4. Only assemblages relevant to peridotite compositions, with various amounts of water, are shown

Mg-sursassite stability in relation to the stabilities of chlorite and phase A

Figure 6 shows a summary of the phase relations for Mg-sursassite, phase A, chlorite, forsterite, enstatite, pyrope and water in the system MASH (peridotite + water). Over the area of the diagram, water is either tied up in chlorite, Mg-sursassite or phase A, or is present as a free fluid phase. Three reactions govern the stability of Mg-sursassite at low water contents. The high- and low-pressure stabilities of Mg-sursassite are determined by reactions (6) and (3), respectively. These are both vapour-absent reactions. With increasing temperature, the stability of Mg-sursassite is defined by the stability of the pyrope-vapour tie-line in reaction (1). Reaction (4) is also important because it provides a mechanism for the transfer of water from chlorite-bearing to Mg-sursassite-bearing assemblages. For slightly higher water contents, Mg-sursassite and chlorite can coexist together in area 6 of the web shown in Fig. 1. Therefore, the upper pressure stability of chlorite below 670 °C is defined by either reaction (3) or (4), dependent on the bulk water content.

In the ultramafic component of a subducting slab, the transfer of water from chlorite to Mg-sursassite to phase A provides a mechanism for the deep subduction of significant amounts of water, providing the P–T path

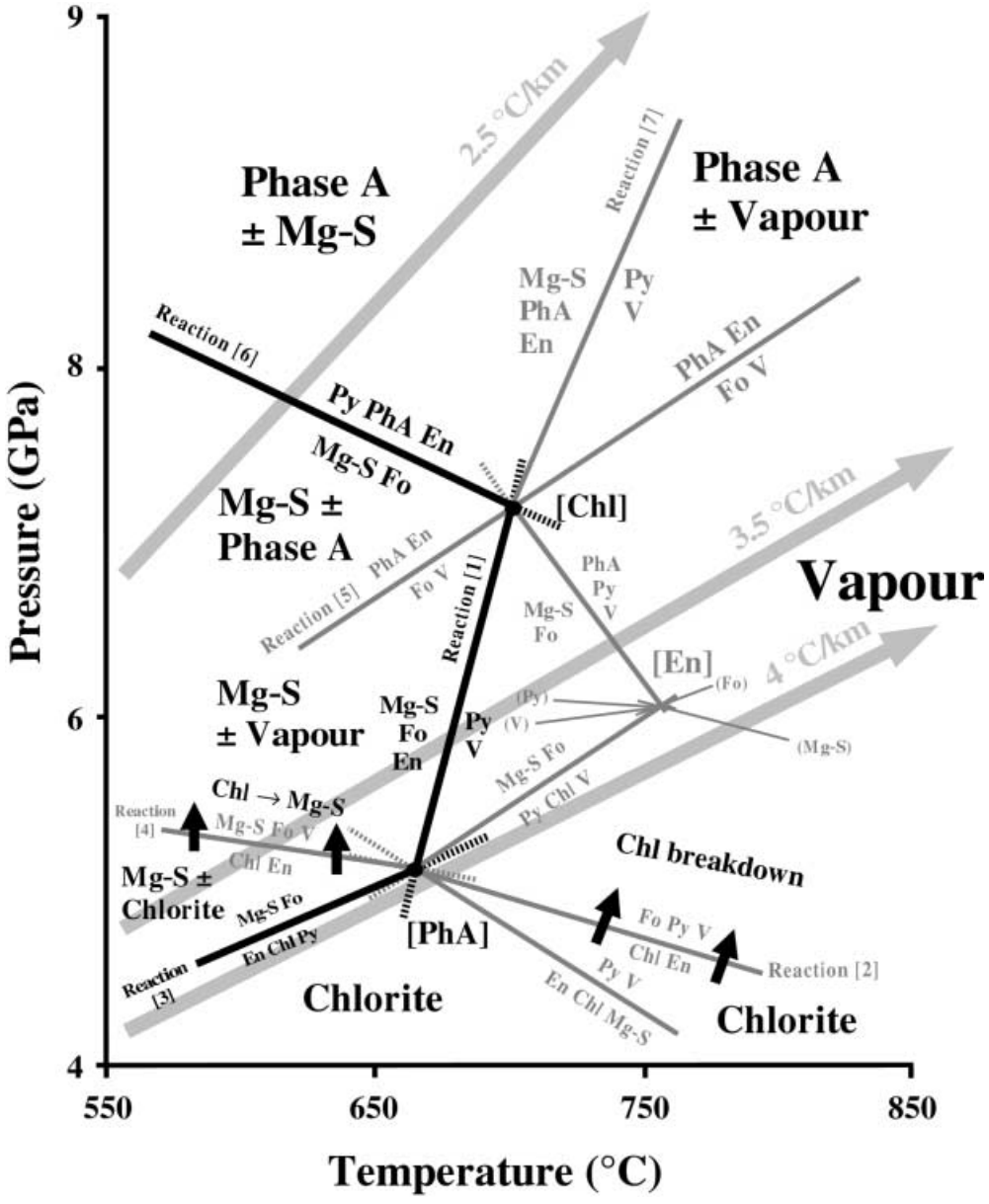

Fig. 6 Schreinemaker's web, with schematic P–T axes, summarising information on the phase relations of Mg-sursassite in the system MASH (peridotite + V). Reactions determining the stability of Mg-sursassite are shown in *black*. *Arrows* indicate important reactions determining chlorite stability and the formation of Mg-sursassite in the subducting slab. *Text in large bold font* indicates the stable hydrous phase(s). Linear geotherms (calculated assuming 1 kbar = 3.33 km) are shown as *light grey arrows*

described by the material lies on the low temperature side of reaction (1). At higher temperatures, breakdown of chlorite via reaction (2) will lead to complete dehydration and the formation of the anhydrous assemblage pyrope + forsterite + enstatite. The position of reaction (1) determined in this study is between 680 and 700 °C. Most previous studies of hydrous phase stability in peridotite have been conducted in the system MSH. In this system, water can only be transported beyond 6 GPa if it can be transferred from antigorite to phase A (Mysen et al. 1998); this reaction occurs only at much lower temperatures (below 600 °C). For more realistic, higher temperature P–T paths for the subducting slab, complete dehydration of the subducting slab will therefore occur. However, the present results demonstrate that in the system MASH, water will be incorporated in hydrous phases up to temperatures of 700 °C. This is a direct result of the stability of Mg-sursassite in the system, which overlaps the stabilities of hydrous phases such as chlorite (and antigorite) towards lower pressures, and phase A at higher pressures. Therefore, although the stability field of Mg-sursassite in peridotite compositions is reduced significantly from its stability in the system MASH as defined by Fockenberg (1998), it can potentially play a pivotal role in water transportation in subduction zones. The presence of Mg-sursassite-bearing assemblages increases the likelihood of the deep subduction of significant quantities of water.

Acknowledgements This work was conducted as part of a PhD thesis at the University of Manchester. Financial support for the project was provided by NERC studentship GT4/97/198/ES. I would like to thank Giles Droop for helpful comments, and Bernd Wunder, Peter Ulmer and Thomas Gottschalk for prompt and thorough reviews.

References

Artioli G, Fumagalli P, Poli S (1999) The crystal structure of $Mg_8(Mg_2Al_2)Al_8Si_{12}(O,OH)_{56}$ pumpellyite and its relevance in ultramafic systems at high pressure. Am Mineral 84:1906–1914

Bohlen SR, Boettcher AL (1982) The quartz–coesite transformation: a precise determination and the effects of other components. J Geophys Res 87:7073–7078

Boyd FR, England JL (1960) Apparatus for phase-equilibrium measurements at pressures up to kilobars and temperatures up to 1,750 °C. J Geophys Res 65:741–748

Chinnery NJ, Pawley AR, Clark SM (1999) In-situ observation of the formation of 10 Å phase from talc + H_2O at mantle pressures and temperatures. Science 286:940–942

Fockenberg T (1998) An experimental study of the pressure–temperature stability of MgMgAl-pumpellyite in the system MgO–Al_2O_3–SiO_2–H_2O. Am Mineral 83:220–227

Gottschalk M, Fockenberg T, Grevel K-D, Wunder B, Wirth R, Schreyer W, Maresch W (2000) Crystal structure of the high-pressure phase $Mg_4(MgAl)Al_4[Si_6O_{21}/(OH)_7]$: an analogue of sursassite. Eur J Mineral 12:935–945

Holland TJB, Redfern SAT (1997) Unit cell refinement from powder diffraction data: the use of regression diagnostics. Mineral Mag 61:65–77

Irifune T, Kubo N, Isshiki M, Yamasaki Y (1998) Phase transformations in serpentine and transportation of water into the lower mantle. Geophys Res Lett 25:203–206

Kawamoto T, Leinenweber K, Hervig RL, Holloway JR (1995) Stability of hydrous minerals in H_2O-saturated KLB-1 peridotite up to 15 GPa. In: Farley KA (ed) Volatiles in the earth and solar system. American Institute of Physics, New York, pp 229–239

Liu L-G (1986) Phase transformations in serpentine at high pressures and temperatures and implications for subducting lithosphere. Phys Chem Mineral 42:252–262

Liu L-G (1989) Stability fields of Mg-pumpellyite composition at high pressures and temperatures. Geophys Res Lett 16:847–849

Luth RW (1995) Is phase A relevant to the Earth's mantle? Geochim Cosmochim Acta 59:679–682

Mysen BO, Ulmer P, Konzett J, Schmidt MW (1998) The upper mantle near convergent plate boundaries. In: Hemley RJ (Ed) Ultra-high pressure mineralogy: physics and chemistry of the Earth's deep interior. Rev Mineral 37:97–138

Pawley AR (2000) Stability of clinohumite in the system MgO–SiO_2–H_2O. Contrib Mineral Petrol 138:284–291

Pawley AR, Wood BJ (1995) The low-pressure stability of phase A, $Mg_7SiO_2O_8(OH)_6$. Contrib Mineral Petrol 124:90–97

Ringwood AE, Major A (1967) High-pressure reconnaissance investigations in the system Mg_2SiO_4–MgO–SiO_2. Earth Planet Sci Lett 2:130–133

Schiffman P, Liou JG (1980) Synthesis and stability relations of Mg–Al pumpellyite, $Ca_5Al_5MgSi_6O_{21}(OH)_7$. J Petrol 21:441–474

Schreyer W (1988) Experimental studies on metamorphism of crustal rocks under mantle pressures. Mineral Mag 52:1–26

Schreyer W, Maresch WV, Medenbach O, Baller T (1986) Calcium-free pumpellyite, a new synthetic hydrous Mg–Al silicate formed at high pressures. Nature 321:510–511

Schreyer W, Maresch WV, Baller T (1991) A new hydrous, high-pressure phase with a pumpellyite structure in the system MgO–Al_2O_3–SiO_2–H_2O. In: Perchuk LL (ed) Progress in metamorphic and magmatic petrology. Cambridge University Press, Cambridge, pp 47–64

Shinmei T, Tomioka N, Fujino K, Kuroda K, Irifune T (1999) In situ X-ray diffraction study of enstatite up to 12 GPa and 1,473 K and equations of state. Am Mineral 84:1588–1594

Susaki J, Akaogi M, Akimoto S, Shimomura O (1985) Garnetndash;perovskite transformation in $CaGeO_3$-in situ X-ray measurements using synchrotron radiation. Geophys Res Lett 12:729–732

Walker D (1991) Lubrication, gasketing and precision in multianvil experiments. Am Mineral 76:1092–1100

Walker D, Carpenter MA, Hitch CM (1990) Some simplifications to multianvil devices for high pressure experiments. Am Mineral 75:1020–1028

Wunder B (1998) Equilibrium experiments in the system MgO–SiO_2–H_2O (MSH): stability fields of clinohumite-OH $[Mg_9Si_4O_{16}(OH)_2]$, chondrodite-OH $[Mg_5Si_2O_8(OH)_2]$ and phase A $[Mg_7Si_2O_8(OH)_6]$. Contrib Mineral Petrol 132:111–120

Wunder B, Rubie DC, Ross CR, Medenbach O, Seifert F, Schreyer W (1993) Synthesis, stability and properties of $Al_2SiO_4(OH)_2$: a fully hydrated analogue of topaz. Am Mineral 78:285–297

Yagi T, Akimoto S (1976) Direct determination of coesite–stishovite transition by in-situ X-ray measurements. Tectonophysics 35:259–270